Appl. Chem. Eng., Vol. 30, No. 1, February 2019, 11-16
https://doi.org/10.14478/ace.2018.1090

Review

수퍼커패시터용 니켈/트리메식 산 기반 금속-유기구조체 전극의 전기화학적 거동에 열처리 온도가 미치는 효과

김정현*,** · 정용주*** · 김 석*,†

*부산대학교 화공 생명공학부, **삼성전자 LED사업부, ***한국기술교육대학교 화학공학과
(2018년 8월 31일 접수, 2018년 9월 28일 심사, 2018년 10월 23일 채택)

Effect of Thermal Treatment Temperature on Electrochemical Behaviors of Ni/trimesic Acid-based Metal Organic Frameworks Electrodes for Supercapacitors

Jeonghyun Kim*,, Yongju Jung***, and Seok Kim*,†**

Department. of Chemical and Biochemical Engineering, Pusan National University, 2, Busandaehak-ro 63, Geumjeong-gu, Busan 46241, South Korea
**LED Business, Samsung Electronics, 1, Samsung-ro, Giheung-gu, Yongin-si, Gyeonggi-do 17113, South Korea*
***Department. of Chemical Engineering, Korea University of Technology and Education (KOREATECH), Cheonan, Chungnam 31253, South Korea*
(Received August 31, 2018; Revised September 28, 2018; Accepted October 23, 2018)

Abstract

Ni-benzene-1,3,5-tricarboxylic acid based metal organic frameworks were successfully synthesized by hydrothermal method and thermally treated at various temperature. The electrochemical performance of composites was investigated using cyclic voltammetry, galvanostatic charge-discharge, and electrochemical impedance spectroscopy. Among all prepared composites, the samples annealed at 250 ℃ showed the highest capacitance with a low resistance, and high cycle stability. It was possible to obtain the low electrical resistance and high electric conductivity of the electrode by improved microstructure and morphology after the thermal annealing at 250 ℃. The samples annealed at 250 ℃ also displayed the maximum specific capacitance with a value of 953 Fg^{-1} at a current density of 0.66 A/g^{-1} in 6 M KOH electrolyte. Moreover, a 86.4% of the initial specific capacitance of the composite was maintained after 3,000 times charge-discharge cycle tests. Based on these properties, it can be concluded that the composite could be applied as potential supercapacitor electrode materials.

***Keywords**: Metal-organic framework, Hydrothermal method, Capacitance, Electrode, Supercapacitor*

1. Introduction

Fossil fuels, which account for about 80% of the total energy, are facing a crisis of depletion at a rapid rate[1,2]. Many countries have been searching the next generation of energy sources to meet increasing energy demand and to reduce air pollutants, which are the main cause of the greenhouse effect. The real challenge is energy storage technology. Of the many energy storage devices, supercapacitors play an important role in hybrid electric vehicles and portable electronic equipment because of their high power density, cycle stability, high reliability, and fast charge/discharge characteristics[3-6]. These supercapacitors have a higher energy density than conventional capacitors, making it possible to apply them to various fields such as memory back-up devices, electrical vehicles, and industrial power supplies[7-12].

As an one model of energy storage devices, there is an electric double layer capacitor (EDLC) that stores charge at the interface of the electrode and the electrolyte through electrostatic force. The other one is the pseudocapacitor, which stores a charge, is a device that stores charge based on the reversible redox reaction on the surface.

Materials such as carbon-based materials, transition metal oxides/hydroxides, and conductive polymers have been used for manufacturing electrode materials used as such supercapacitors[13]. In general, carbon-based materials store a large amount of electric charge on the electrode surface based on the EDLC principle. However, due to the electrostatic surface charging mechanism and the inherent problem of agglomeration which is the limit of the carbon-based material, the low specific capacitance does not meet the required level of an electric device having a sufficient energy density, and studies are under way[14]. On the other hand, materials such as transition metal ox-

† Corresponding Author: Pusan National University, Department. of Chemical and Biochemical Engineering, 2, Busandaehak-ro 63, Geumjeong-gu, Busan 46241, South Korea
Tel: +82-51-510-3874 e-mail: seokkim@pusan.ac.kr

pISSN: 1225-0112 eISSN: 2288-4505

ide/hydroxide or conductive polymer rapidly perform charge storage through a reversible Faradaic oxidation/reduction reaction. Therefore, pseudocapacitors usually show higher specific capacitance than EDLCs [13-17]. However, intrinsic high resistance and low cycle stability have limited the use of pure transition metal oxide as a supercapacitor electrode. As a result, securing new technologies to solve these deficiencies of electrode in supercapacitors and developing clean materials to meet new requirements is highly desirable and of practically valuable.

On the other hand, metal-organic frameworks (MOFs), which is emerging as a new type of porous material, have been widely recognized as supercapacitor electrode materials because of their wide specific surface area, controllable pore size, and incorporated redox metal centers. Despite the usage of MOF materials in the development of supercapacitors was an important prospect, only few electrodes have been studied as a function of the annealing temperature of the Ni-MOF for supercapacitors. Herein, we report a synthesis and electrochemical characterization of Ni-BTC MOFs prepared by a hydrothermal method. This study structurally confirmed the temperature - dependent changes in the phase transition of nickel corresponding to the metal center and the organic ligands forming the MOFs. The effect of thermal treatment temperature is evaluated by studying the structural characteristic and electrochemical properties of the Ni-BTC MOFs. The optimum temperature of Ni-BTC MOFs for thermal annealing also had been determined.

2. Experimental

2.1. Synthesis of Ni-BTC MOFs

All chemicals used in this experiment were of analytical grade and were used without further purification. Two solutions of 20 mmol of Nicke l(II) nitrate hexahydrate ($Ni(NO_3)_2 \cdot 6H_2O$) dissolved in 40 mL deionized water and 10 mmol of Trimesic acid (H3BTC, benzene-1,3,5-tricarboxylic acid) dissolved in 40 mL dimethylformamide (DMF) were prepared separately. Two solutions were loaded into the Teflon liner and fully mixed.

Solution mixtures was heated at 160 ℃ for 48 h in a convection oven. The Teflon liner was then cooled to room temperature. MOF crystals were filtered and washed with deionized water and ethanol successively and freeze-dried to obtain the final product.

2.2. Preparation of thermally treated Ni-BTC MOFs

The obtained Ni-BTC MOF was transferred to a heating furnace and heated to various temperatures. This step was conducted at various temperature (150~650 ℃) under air atmosphere using a raising rate of 1 ℃min^{-1}. The obtained samples were named as N150, N250, N350, N450, N550 and N650 according to treatment temperature respectively. For comparison, we prepared a sample without heat treatment, and is was named as No HT.

2.3. Characterization methods

The microstructures of Ni-BTC MOFs were analyzed by field emission scanning electron microscopy (FE-SEM, Carl Zeiss, Supra 25) and transmission electron microscopy (H-7600 (HITACHI)). X-ray diffraction (XRD) analysis of materials were measured on Empyrean series2 X-ray diffractometer with Cu-Kα radiation (λ = 1.5406 Å). The Fourier transform infrared (FT-IR) spectra were recorded on Perkin Elmer FT-IR Spectrum two in the range of 650-4,000 cm^{-1}. Specific surface area measurement was done by Brunauer-Emmett-Teller (BET, Micromeritics ASAP 2020).

2.4. Electrochemical characterization

All electrochemical results were measured with a three electrode system from Iviumstat (Ivium Technologies, Netherlands). The working electrode was prepared in the following method. The prepared composite, carbon black (Super-P, Alfa-aesar), and polyvinylidone fluoride (PVDF) were mixed in an agate mortar at a ratio of 85 : 10 : 5 under *N*-methyl-2-pyrrolidene (NMP) solvent. The homogeneously mixed slurry is coated on a nickel foam current collector (1 cm × 1 cm) and dried in a vacuum oven at 80 ℃ for 12 h. A saturated calomel electrode (SCE) and Pt wires were used as reference and counter electrodes, respectively, and measurements were made in a 6M aqueous KOH solution. The cyclic voltammograms (CV) were acquired between -0.15 to 0.4 V at different scan rates of 5, 10, 20, 30 and 50 mVs^{-1}. Galvanostatic charge-discharge curves were acquired in the same potential range at a current density of 0.66, 1, 2, 2.5, 3 and 5 Ag^{-1}. Electrochemical impedance spectroscopy (EIS) measurements were performed in the frequency range of 100,000 Hz to 0.01 Hz at open circuit potential with an alternating current (AC) perturbation of 5 mV. The specific capacitance of the composites was calculated from the GCD curves using the following equation:

$$C = \frac{I \times \triangle t}{m \times \triangle V} \quad (1)$$

where I is the response current density (A g^{-1}), $\triangle t$ is discharge time (sec), m is the mass of the composite in the electrodes (g), and $\triangle V$ is the difference between the highest and lowest potential (V). The electrochemical impedance spectroscopy (EIS) measurements were performed in the frequency range from 100,000 Hz to 0.01 Hz at open circuit potential with an alternating current (AC) perturbation of 5 mV.

3. Results and Discussion

3.1. Microstructural characterization

The synthesis of Ni-BTC MOF is roughly divided into two processes as shown in Figure 1. First, a crystalline Ni-BTC MOF is obtained through a hydrothermal synthesis reaction, and the particle shape can be confirmed later by referring to Figure 4. Finally, the thermal treatment for Ni-BTC MOF particles were performed by heat treatment process by changing temperatures.

Figure 2 shows the X-ray diffraction (XRD) patterns of the prepared composites. It can be seen from the XRD pattern that the structure of the MOF is maintained as it is for the heat-treated samples between

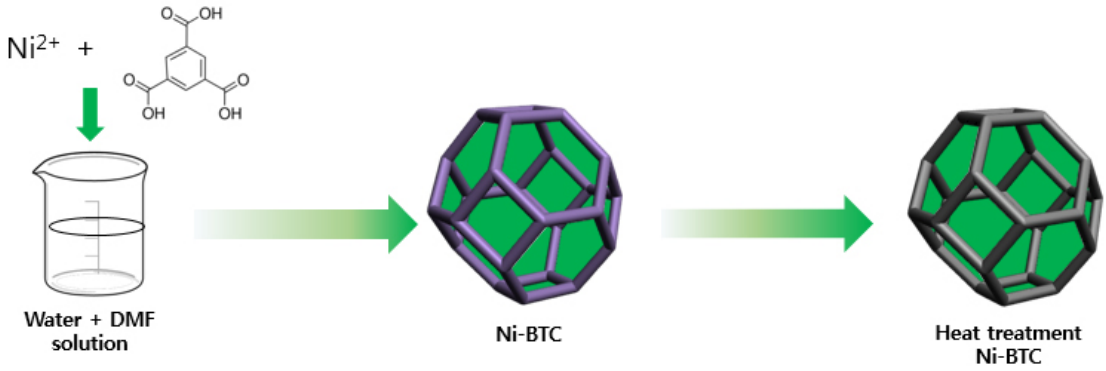

Figure 1. Schematic representation of the preparation process of Ni-BTC MOFs.

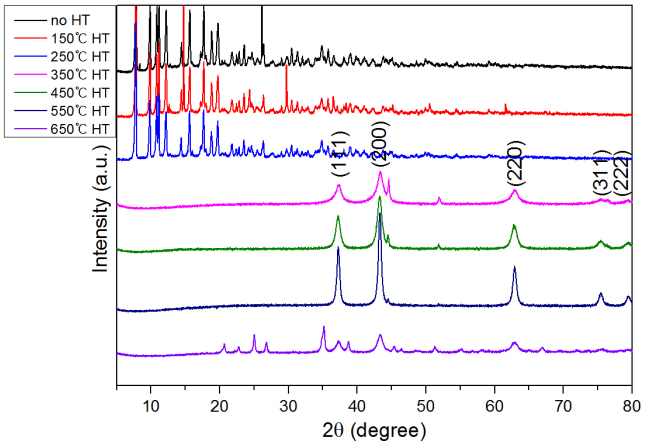

Figure 2. X-ray diffraction patterns of various heat treatment Ni-BTC MOFs.

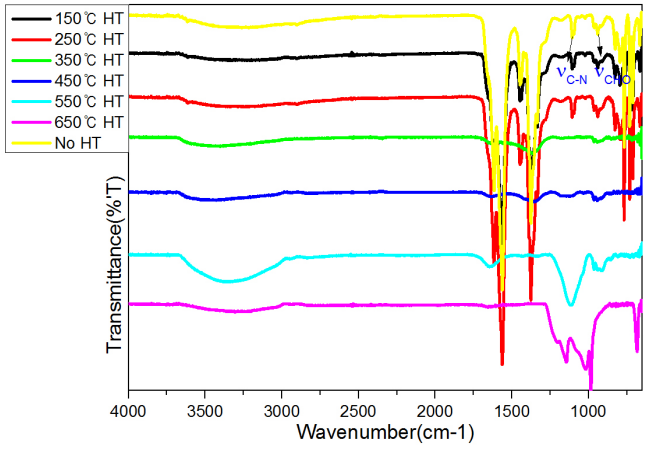

Figure 3. FT-IR spectra of various thermally treated Ni-BTC MOFs.

25 ℃ and 250 ℃. However, it can be confirmed that the structure of the MOF is collapsed for the samples of 350 ℃ or higher temperature annealing. Their crystalline peak appearance were quite different with that for the heat-treated samples between 25 ℃ and 250 ℃. It can be seen that the separation or removal of the DMF molecules in the MOF structure occurs at around 300 ℃[18]. It could be said that the crystalline structure of Ni-BTC MOFs had been developed and stabilized under the thermal annealing at temperature of 250 ℃.

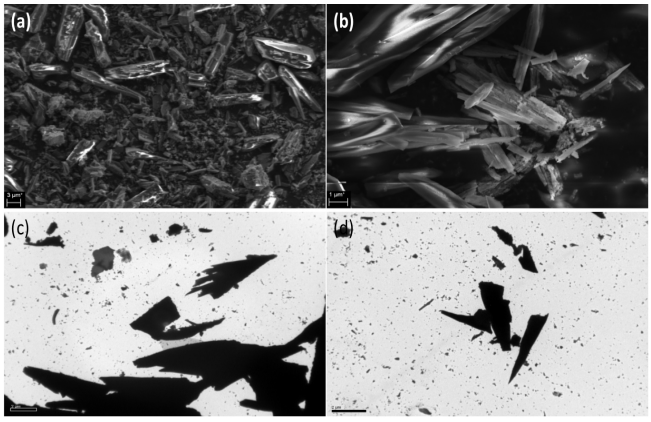

Figure 4. (a), (b) FE-SEM and (c), (d) TEM images of N250 sample.

FT-IR spectroscopy was used to analyze the functional groups and microstructure characteristics. Figure 3 shows the FT-IR spectrums of various sample of Ni-BTC MOFs recorded in the range of 4,000-650 cm^{-1}. They show similar IR absorption patterns with Ni ion coordinated COO moiety in the range of 1,350-1,650 cm^{-1}[19], and C-N and CN-CHO vibrational frequencies observed at 1,103 and 936 cm^{-1} indicated the presence of Ni coordinating to DMF molecules. The C=O band at 1,600 cm^{-1} in FT-IR spectra of Ni-BTCs represented the amide group from DMF. As with the XRD pattern, the FT-IR results show that the MOF structure collapses result in the disappearance of the peaks of C-N and CN-CHO for samples above 350 ℃.

Morphology analysis of the composite surface was done through field emission scanning electron microscopy (FE-SEM) and transmission electron microscopy (TEM) images. Figure 4 (a), (b) shows the FE-SEM images and Figure 4 (c), (d) shows the TEM images of the as-prepared composites. The Ni-BTC MOF crystals are found to have well-regulated particle size of 1-10 μm. The particle of the Ni-BTC MOF showed the rod-like appearance and the some parts are aggregated from the primary particle. However, we could say the surface is quite smooth and the ordered structure of porous materials. BET surface areas of the Ni-BTC MOF crystals measured by N_2 gas adsorption isotherms were in the order of 900 m^2/g. This is quite similar to the previous result[20]. The measured specific surface areas of

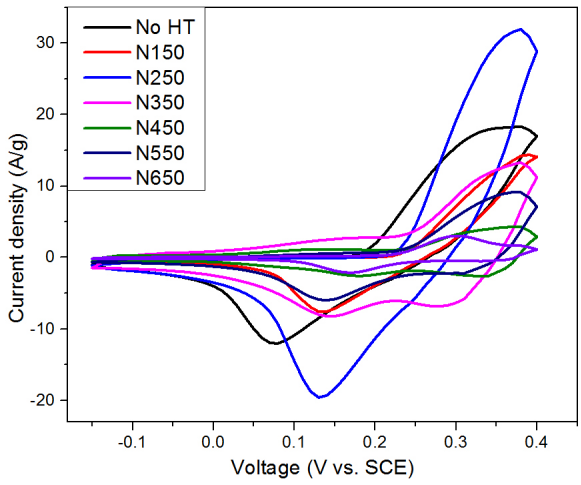

Figure 5. CV curves of various heat treatment Ni-BTC MOF at a scan rates 30 mVs^{-1}.

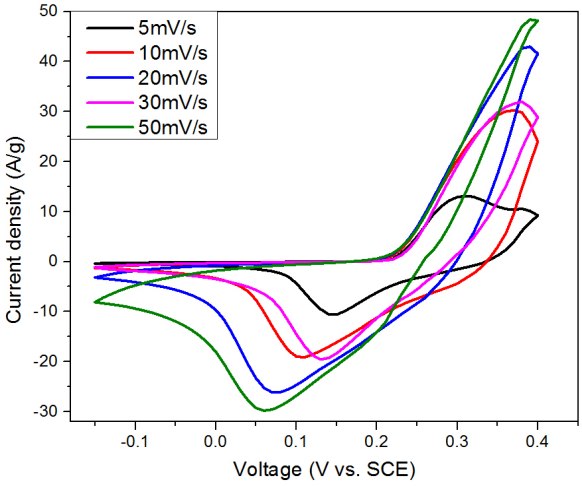

Figure 6. CV curves of N250 at various scan rates (5, 10, 20, 30, and 50 mVs^{-1}).

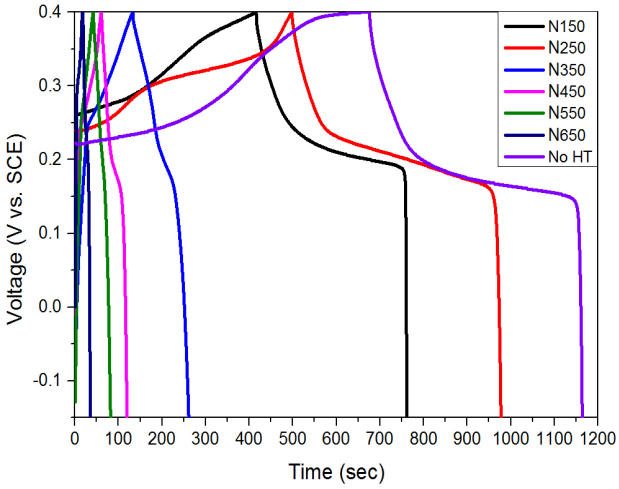

Figure 7. Galvanostatic charge-discharge curves of various heat treatment Ni-BTC MOF at a current density of 1 Ag^{-1}.

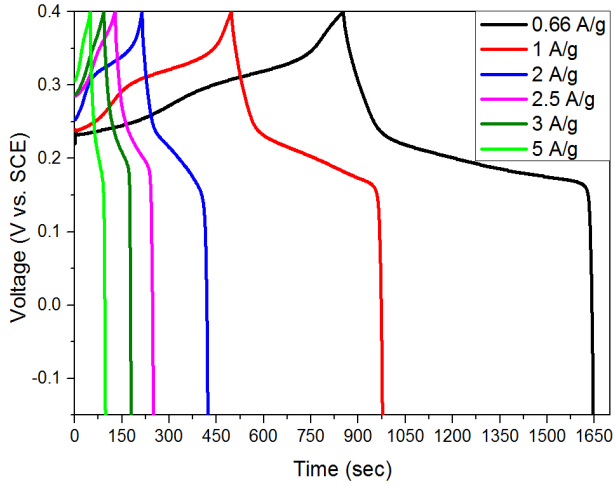

Figure 8. Galvanostatic charge-discharge curves of N250 at various current density (0.66, 1, 2, 3, and 5 Ag^{-1}).

N150, N250, N350, N450, N550, and N650 samples are 840, 860, 812, 798, 788, 756 m^2/g, respectively. By increasing the heat treatment temperature, the surface area had been gradually decreased probably due to some agglomeration and change of microstructure.

3.2. Electrochemical performance

The electrochemical performance of the prepared electrode was measured by cyclic voltammetry (CV), galvanostatic charge-discharge (GCD), and electrochemical impedance spectroscopy (EIS). Figure 5 shows the CV curves of the various temperature heat treatment Ni-BTC MOF at scan rate 30 mVs^{-1} in the potential range of -0.15 to 0.4 V (*vs.* SCE) in 6 M KOH electrolyte. A couple of redox peaks are observed within the potential range from -0.15 to 0.4 V. Two possible reactions can occur with a quasi-reversible redox reaction during a potential sweep[21]:

$$Ni(II)s + OH^- \leftrightarrow Ni(II)(OH)_{ad} + e^- \quad (2)$$

$$Ni(II)(OH)_{ad} \leftrightarrow Ni(III)(OH)_{ad} + e^- \quad (3)$$

The anodic peak is due to the oxidation of Ni(II) to Ni(III) and the cathodic peak is for the reverse reduction process[22]. It indicates that the capacitance mainly results from the pseudo-capacitive capacitance, which is based on a redox mechanism. It should be noted that with the sweep rate increases, the increment in the area of the CV and its current response is observed. This indicates that the nickel-based MOF is appropriate for fast reversible Faradaic reactions.

Figure 6 shows the changes of the redox peaks of the N250 in the CV curves at different scan rates in the range 5-50 mVs^{-1}. At low scan rates, ion movement occurs at both the inner and outer surfaces of the composites. At high scan rates, however, due to structural limitations of pore structures, the ion exchange reaction occurs only on the outer surface of the electrode.

Figure 7 shows the constant current charge-discharge curve of the composite material. Charge-discharge analysis was carried out at a po-

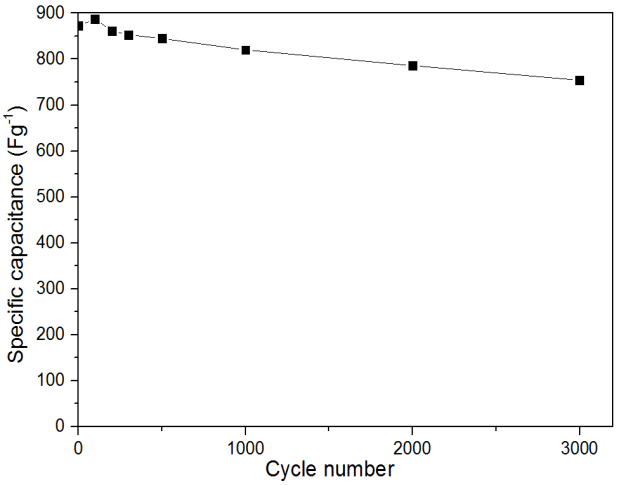

Figure 9. Cycling performances of N250.

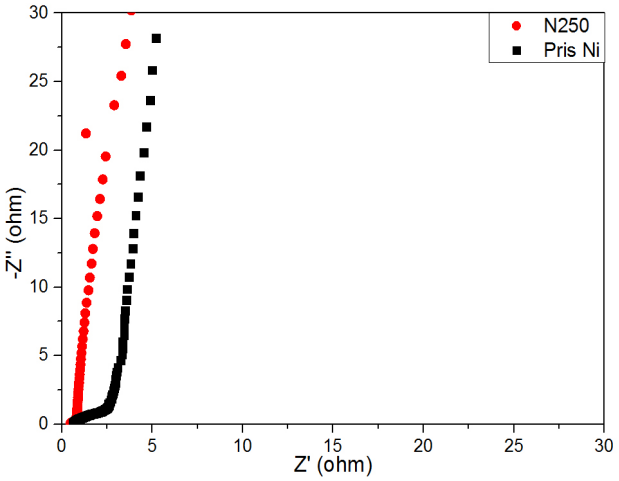

Figure 10. Nyquist plots of N250 and Pris Ni (pristine Ni-BTC MOFs).

tential range of -0.15 V to 0.4 V at a current density of 1 A/g. Two voltage stages are observed during the discharge process. The first stage is the voltage drop from 0.4 V to 0.23 V. It can be seen that the shape of the ideal line is close to that of the ideal line, which can be attributed to the electric double layer capacitance effect. The second slow potential decay from 0.28 V to 0.18 V occurs during the redox process in the metal of the electrode, which explains pseudo-capacitive performance. $Ni(OH)_2$ crystals having a high capacitance are expected to be formed at 90 ℃[20]. Also, it can be seen that the residues are removed in the process of increasing to 250 ℃, and the capacitance is secured by securing the crytallinity[23,24]. Also, it can be seen that when the temperature exceeds 250 ℃, the capacitance drops sharply. This result is due to the fact that the organic ligand of the MOF substance is decomposed at a temperature of 250 ℃ or more and cannot have the unique structure of the MOF material, and thus the pseudo-capacitance cannot be secured[18]. From the curves, that the charge storage capacity of the N250 is evidently higher than that of the remaining samples. The calculated specific capacitance of No HT, N150, N250, N350, N450, N550, and N650 samples are 862, 596.4, 873, 235, 109, 73, and 33 Fg^{-1}, respectively at a current density of 1 Ag^{-1}. As well known, the capacitance value is highly dependent on the specific surface area of samples. However, N250 showed the highest capacitance value, although the sample did not show the largest value in surface area. It is thought that capacitance is mainly related to the surface area. However, the other factor such as surface element composition and electrical conduction also could influence the capacitance value[24].

Figure 8 shows the charge-discharge curves of the N250 at a various current density. The maximum specific capacitance of the N250 was 953 Fg^{-1} at 0.66 Ag^{-1}. As the discharge current density increases from 0.66 Ag^{-1} to 5 Ag^{-1}, a large voltage drop is observed, and finally the capacitance decreases from 953 Fg^{-1} to 240 Fg^{-1}. The reduction in capacitance is caused by the presence of an internal active site that is unable to fully perform redox transitions at high current densities. This phenomenon can be explained with reference to OH^- ion diffusion during the charge and discharge of the electrode. At relatively high rates of high current density, OH- ions must be rapidly inserted at the interface between the electrode and the electrolyte, but non-uniformity of the OH- ions due to undesirable accessibility of the ions in the diffusion process cannot meet this requirement[25].

High lifetime stability is an important requirement for high-performance supercapacitor electrode materials. Figure 9 shows the cycle performance of the prepared composites in the range of -0.15 V to 0.4 V (*vs*. SCE) for 3,000 cycles at a 1 Ag^{-1}. As shown in Figure 9, it was confirmed that 93.9% of the initial value was maintained for the first 1,000 cycles, and it was confirmed that the cycle characteristic of 90.0% was stable even for 2,000 cycles. In the range of 2,000 to 3,000 cycles, there was a slight decrease of 86.4% of the initial value, which was attributed to the structural collapse of Ni-MOF in the process of OH^- ion redox reaction at the interface between the electrode and the electrolyte.

Figure 10 shows the Nyquist plot of the EIS of the prepared composites. From the plot, Z' in the coordinate shows the ohmic characteristic of the electrode and the imaginary part corresponding to -Z'' shows the capacitance characteristic. The semicircle at high frequencies means the equivalent series resistance (ESR) of the electrodes, and the straight line in the low frequency region represents diffusion resistance and ion diffusion with the electrolyte. The closer to the vertical in the straight line part, the faster the ion diffusion between the electrolyte and the electrode leads to the charge transfer, which is an ideal behavior for the electrode[26]. It can be seen that the N250 sample shows a higher straight line than the pristine Ni-BTC MOFs, which means that it is a more suitable material as a supercapacitor electrode material. In addition, as can be seen from the difference of semi-circle size of the Nyquist plot, it can be confirmed that the resistance value is lower because the semicircle is smaller than the pristine Ni-BTC MOFs. Lower ESR values show that the electrical conductance is increased through the organic ligands of Ni-BTC MOFs and the easily accessible ion transport path, resulting in lower electrode resistance and ion transfer rate. These results were similar trend with the analysis of CV and GCD graphs.

4. Conclusions

We have demonstrated the preparation of Ni-BTC MOFs using a hydrothermal method and investigated the correlation of structural and electrochemical performance with annealing temperature. The N250 sample is effectively improved for the super-capacitive performance when it is compared to the pristine Ni-BTC MOFs. It is believed that $Ni(OH)_2$, which has a high capacitance materials at 90 ℃, was formed and developed during the process of raising the temperature to 250 ℃, it was possible to obtain low electrical resistance and high electric conductivity of the electrode by improved microstructure and the better surface area for electrode reaction. The N250 showed enhanced electrochemical properties such as specific capacitance, rate capability and cycle performance. Especially, the N250 had the maximum specific capacitance of 953 Fg^{-1} at 0.66 Ag^{-1} current density, which was higher compared to that (862 Fg^{-1}) for the No HT. In addition, the cycle performance of the N250 sample (~86.4% over 3,000 cycles compared to the initial value) has been greatly improved. Considering the excellent capacity and electrochemical properties of these composites, these composites are considered as promising materials for high performance supercapacitors.

Acknowledgement

This work was supported by the Individual Basic Science & Engineering Research Program through the National Research Foundation (NRF) of Korea, and funded by the MOE (Ministry of Education), Korea (Grant No. NRF-2018R1D1A1B07047857).

References

1. M. Hoel and S. Kverndokk, Depletion of fossil fuels and the impacts of global warming, *Resour. Energy Econ.*, **18**, 115-136 (1996).
2. S. Shafiee and E. Topal, When will fossil fuel reserves be diminished?, *Energy Policy*, **37**, 181-189 (2009).
3. M. F. El-Kady, V. Strong, S. Dubin, and R. B. Kaner, Laser scribing of high-performance and flexible graphene-based electrochemical capacitors, *Science*, **335**, 1326-1330 (2012).
4. J. R. Miller and P. Simon, Electrochemical capacitors for energy management, *Science*, **321**, 651-652 (2008).
5. P. Simon and Y. Gogotsi, Materials for electrochemical capacitors, *Nat. Mater.*, **7**, 845-854 (2008).
6. J. Balamurugan, T. D. Thanh, N. H. Kim, and J. H. Lee, Facile synthesis of 3D hierarchical N-doped graphene nanosheet/cobalt encapsulated carbon nanotubes for high energy density asymmetric supercapacitors, *J. Mater. Chem. A*, **4**, 9555-9565 (2016).
7. J. Kim, S. J. Park, and S. Kim, Capacitance behaviors of polyaniline/graphene nanosheet composites prepared by aniline chemical Polymerization, *Carbon Lett.*, **14**(1), 51-54 (2013).
8. J. Kim, S. C. Byun, S. Chung, and S. Kim, Preparation and capacitance properties of graphene based composite electrodes containing various inorganic metal oxides, *Carbon Lett.*, **25**, 14-24 (2018).
9. J. E. Kim and S. Kim, Preparation and electrochemical analysis of graphene/polyaniline composites prepared by aniline polymerization, *Res. Chem. Intermediates*, **40**(7), 2519-2525 (2014).
10. J. E. Kim, Y. Kim, S.-J. Park, Y. Jung, and S. Kim, Preparation and electrochemical analysis of graphene nanosheets/nickel hydroxide composite electrodes containing carbon nanotubes, *J. Ind. Eng. Chem.*, **36**, 139-146 (2016).
11. L. H. Bao, J. F. Zang, and X. D. Li, Flexible Zn_2SnO_4/MnO_2 core/shell nanocable-carbon microfiber hybrid composites for high-performance supercapacitor electrodes, *Nano Lett.*, **11**(3), 1215-1220 (2011).
12. H. M. Yoo, G. Y. Heo, and S. J. Park, Effect of crystallinity on the electrochemical properties of carbon black electrodes, *Carbon Lett.*, **12**(4), 252-255 (2011).
13. G. P. Wang, L. Zhang, and J. J. Zhang, A review of electrode materials for electrochemical supercapacitors, *Chem. Soc. Rev.*, **41**, 797-828 (2012).
14. X. H. Lu, Y. X. Zeng, M. H. Yu, T. Zhai, C. L. Liang, S. L. Xie, M. S. Balogun, and Y. X. Tong, Oxygen-deficient hematite nanorods as high-performance and novel negative electrodes for flexible asymmetric supercapacitors, *Adv. Mater.*, **26**, 3148-3155 (2014).
15. A. S. Arico, P. Bruce, S. Bruno, J. M. Tarascon, and W. V. Schalkwijk, Nanostructured materials for advanced energy conversion and storage devices, *Nat. Mater.*, **4**, 366-377 (2005).
16. M. S. Oh and S. Kim, Synthesis and electrochemical analysis of polyaniline/TiO_2 composites prepared with various molar ratios between aniline monomer and para-toluenesulfonic acid, *Electrochim. Acta*, **78**, 279-285 (2012).
17. M. Oh, S. J. Park, Y. Jung, and S. Kim, Electrochemical properties of polyaniline composite electrodes prepared by in-situ polymerization in titanium dioxide dispersed aqueous solution, *Synth. Met.*, **162**(7-8), 695-701 (2012).
18. F. Israr, D. K. Kim, Y. Kim, and W. Chun, Scope of various solvents and their effects on solvothermal synthesis of Ni-BTC, *Quim. Nova*, **39**, 669-675 (2016).
19. H. Kumagai, Y. Oka, M. A. Tanaka, and K. Inoue, Hydrothermal synthesis and characterization of a two-dimensional nickel (II) complex containing benzenehexacarboxylic acid(mellitic acid), *Inorg. Chim. Acta*, **332**, 176-180 (2002).
20. F. Israr, D. Chun, Y. Kim, and D. K. Kim, High yield synthesis of Ni-BTC metal-organic framework with ultrasonic irradiation: Role of polar aprotic DMF solvent, *Ultrason. Sonochem.*, **31**, 93-101 (2016).
21. L. Kang, S. X. Sun, L. B. Kong, J. W. Lang, and Y. C. Luo, Investigating metal-organic framework as a new pseudo-capacitive material for capacitors, *Chin. Chem. Lett.*, **25**, 957-961 (2014).
22. X. Sun, G. K. Wang, J. Y. Hwang, and J. Lian, Porous nickel oxide nano-sheets for high performance pseudocapacitance materials, *J. Mater. Chem.*, **21**, 16581-16588 (2011).
23. B. R. Shanaj and X. R. John, Effect of calcination time on structural, optical and antimicrobial properties of nickel oxide nanoparticles, *J. Theor. Comput. Sci.*, **3**, 149 (2016).
24. J. Kim, Y. Kim, S. J. Park, Y. Jung, and S. Kim, Preparation and electrochemical analysis of graphene nanosheets/nickel hydroxide composite electrodes containing carbon nanotubes, *J. Ind. Eng. Chem.*, **36**, 139-146 (2016).
25. R. Kotz and M. Carlen, Principles and applications of electrochemical capacitors, *Electrochim. Acta*, **45**(15-16), 2483-2498 (2000).
26. X. Jiang, Y. Ma, J. Li, and W. Huang, Self-assembly of reduced graphene oxide into three-dimensional architecture by divalent ion linkage, *J. Phys. Chem.*, **114**(51), 22462-22465 (2010).